

## Combined three-dimensional lattice Boltzmann method and discrete element method for modelling fluid–particle interactions with experimental assessment

Y. T. Feng<sup>\*,†</sup>, K. Han and D. R. J. Owen

*Civil and Computational Engineering Centre, School of Engineering, Swansea University, SA2 8PP, U.K.*

### SUMMARY

A general algorithmic framework is established in this paper for numerical simulations of three-dimensional fluid–particle interaction problems with a large number of moving particles in turbulent flows using a combined lattice Boltzmann method (LBM) and discrete element method (DEM). In this approach, the fluid field is solved by the extended three-dimensional LBM with the incorporation of the Smagorinsky turbulence model, while particle interactions are modelled by the DEM. The hydrodynamic interactions between fluid and particles are realized through the extension of an existing two-dimensional fluid–particle hydrodynamic interaction scheme. The main computational aspects comprise the lattice Boltzmann formulation for the solution of fluid flows, the incorporation of a large eddy simulation-based turbulence model within the framework of the three-dimensional LBM for turbulent flows, the moving boundary condition for hydrodynamic interactions between fluid and moving particles, and the discrete element modelling of particle–particle interactions. To assess the solution accuracy of the proposed approach, a much simplified laboratory model of vacuum dredging systems for mineral recovery is employed. The numerical results are compared with the experimental data available. It shows that the overall correspondence between numerical results and experimental measurements is good and thus indicates, to a certain extent, the solution accuracy of the proposed methodology. Copyright © 2009 John Wiley & Sons, Ltd.

Received 4 May 2008; Revised 16 April 2009; Accepted 28 May 2009

**KEY WORDS:** lattice Boltzmann method; discrete element method; fluid–particle interactions; moving boundary condition; Smagorinsky turbulence model; experimental assessment

---

\*Correspondence to: Y. T. Feng, Civil and Computational Engineering Centre, School of Engineering, Swansea University, SA2 8PP, U.K.

†E-mail: y.feng@swansea.ac.uk

Contract/grant sponsor: Leverhulme Trust Research Fellowship Award; contract/grant number: RF/9/RFG/2007/0326

## 1. INTRODUCTION

Fluid–particle interaction problems can be found in many scientific and engineering applications, such as particle suspensions, fluidized beds, lubricated transport, sedimentation, fluvial erosion, and geo-mechanical systems including liquefaction and piping. The fundamental physical phenomena involved in these problems are generally not well understood and are often described in an empirical fashion, mainly due to the intricate complexity of the fluid–particle interactions exhibited. The motion of the particles is driven collectively by gravity and the hydrodynamic forces exerted by the fluid, and may also be altered by the interaction between particles. On the other hand, the fluid flow pattern can be greatly affected by the presence of the particles, and is often of a turbulent nature.

The numerical treatment of fluid–particle interaction problems may crucially depend on the size of the particles in relation to the domain/mesh size. For small particle/mesh size ratios, as occur, for example, in fluidised bed applications in which the particle–fluid hydrodynamics is described by the Navier–Stokes equations in the averaged sense based on the local porosity of the fluid cells, while empirical-based drag forces are applied to particles to determine the motion of the particles [1]. However, this solution strategy becomes less accurate when the particle sizes are larger than the mesh size because not sufficient resolution is provided for the fluid field. Thus alternative solution procedures must be sought.

Substantial effort has been invested over recent decades in the development of various finite element-based techniques to model fluid–particle interactions where sufficient resolution of the particle domain is required, see for instance [2]. Although the methodology can be employed to simulate problems involving many particles, it may not be computationally effective when a large number of particles are present due to intensive computations involved in the continuous generation of new adapted meshes to circumvent severe mesh distortion, particularly in the three-dimensional cases.

In recent years, the lattice Boltzmann method (LBM) has attracted considerable research attention and has emerged as an alternative solution technique to the conventional computational fluid dynamics (CFD) methods employing Navier–Stokes equations. It offers various advantages over the Navier–Stokes equations, including high space–time resolution, full scalability on parallel computers, as well as efficient and robust implementation in complex geometries [3]. Another distinct feature of the LBM over the finite volume method and finite element method is the use of an Eulerian grid to represent the flow field. For these reasons, the LBM is ideal for simulating fluid flows in complex geometries, such as the fluid–particle interaction problems considered. Since Ladd's early work [4], the LBM has been widely employed to model fluid–particle interactions, see for instance [5–8]. Furthermore, employing the discrete element method (DEM) to account for particle–particle interactions gives rise to a combined LBM–DEM solution procedure. The explicit time stepping scheme of both the LBM and the DEM makes this combined strategy a competitive numerical tool for the simulation of fluid–particle systems, having potential to be a powerful predictive tool for gaining fundamental insight into many poorly understood physical phenomena.

While the LBM has been well established for laminar flows, turbulence modelling within the framework of the LBM remains a challenge. Recently, limited attempts have been made to incorporate some existing turbulence models into the LBM. The large eddy simulation (LES) procedure with the Smagorinsky sub-grid model [9] is the simplest to apply. The approach assumes that the Reynolds stress tensor is dependent only on the local strain rate. This model is very

convenient in numerical simulations as it leaves the Navier–Stokes equation invariant except for a renormalized turbulent viscosity [10].

In our previous work [11, 12], the coupled LBM–DEM strategy together with the incorporation of the LES with a Smagorinsky sub-grid model has been successfully implemented in the simulation of two-dimensional fluid–particle interaction problems in turbulent flows with regular and irregular-shaped particles.

The objective of this work is to extend the methodologies to three-dimensional situations so that realistic fluid–particle interaction problems with a large number of moving particles in turbulent flows can be effectively simulated. In this coupled numerical framework, the (turbulent) fluid field is solved by the extended LBM with the incorporation of the Smagorinsky turbulence approach, while the particle interaction is modelled by the DEM. In particular, the hydrodynamic interactions between fluid and particles are realized through the three-dimensional generalization of the scheme proposed by Noble and Torczynski [13]. Since both the LBM and DEM are well established, it is crucial to investigate the validity of the three-dimensional extension of Noble and Torczynski's hydrodynamic scheme. Although the three-dimensional scheme has been validated very recently by Strack and Cook [14] for a number of problems involving spheres embedded in laminar fluid flows, no validation has been conducted for problems involving turbulent flows, which is essential for simulating practical particle transport applications. In the present work, in view of the inherent difficulties associated with the conduction of such a validation, a much simplified sample vacuum dredging system for mineral recovery is simulated by the proposed approach, and then the simulated results are compared with the corresponding experimental data available in order to assess, to a certain extent, the accuracy of the whole numerical strategy in general and the hydrodynamic scheme in particular.

The remainder of the paper is arranged as follows. A brief introduction of the three-dimensional LBM and its incorporation with the LES-based Smagorinsky model are given first, followed by a detailed discussion of the modelling of the fluid–particle and particle–particle interactions. Then an assessment is performed where the results of the numerical simulation of a vacuum dredging system are compared with those obtained experimentally.

## 2. THE LBM

In the conventional CFD methods, the macroscopic variables of the fluid field, such as velocity  $\mathbf{v}$  and pressure  $p$ , are obtained by solving the Navier–Stokes equations in space and time. Instead, the LBM does not solve the Navier–Stokes equations directly, but is based on the kinetic gas theory, which simulates fluid flows by tracking the evolution of the single fluid ‘particle’ distribution. Once the distribution function is solved, macroscopic variables of the fluid field can be conveniently calculated from its first two moments.

In the LBM, the problem domain is divided into regular lattice nodes. The fluid is modelled as a group of fluid particles that are allowed to move between the adjacent lattice nodes or stay at rest. During each discrete time step of the simulation, fluid particles move to their nearest lattice nodes along their directions of motion, where they ‘collide’ with other fluid particles that arrive at the same node. The outcome of the collision is determined by solving the kinetic (Boltzmann) equation for the new distribution function at that node and the fluid particle distribution function is updated.

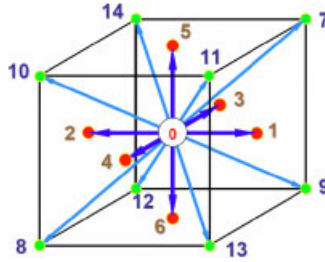


Figure 1. D3Q15 model.

As the relevant literature is very rich (see [15] for a comprehensive review), only essential aspects of the method for the three-dimensional cases are outlined below.

### 2.1. D3Q15 model

The lattice Boltzmann equation with single-relaxation-time approximation introduced by Bhatnagar *et al.* [16] for the collision operator is expressed as

$$f_i(\mathbf{x} + \mathbf{e}_i \Delta t, t + \Delta t) - f_i(\mathbf{x}, t) = -\frac{1}{\tau} [f_i(\mathbf{x}, t) - f_i^{\text{eq}}(\mathbf{x}, t)] \quad (1)$$

where  $f_i$  is the density distribution function with discrete velocity  $\mathbf{e}_i$  along the  $i$ th direction;  $f_i^{\text{eq}}$  is the equilibrium distribution function; and  $\tau$  is the single relaxation time, which controls the rate of approach to equilibrium. The left-hand side of Equation (1) denotes a streaming process for fluid particles, while the right-hand side models the collisions through relaxation.

There are a number of different models available in three-dimensional simulations. The widely adopted D3Q15 model, which is adopted here, uses a cubic lattice with 15 discrete velocity directions. The fluid particles at each lattice node move to their 14 neighbouring nodes with discrete velocities  $\mathbf{e}_i$ , ( $i = 1, \dots, 14$ ), as shown in Figure 1. A proportion of the particles remain at the node, which is equivalent to moving with a zero velocity  $\mathbf{e}_0$ . With reference to the numbering system in Figure 1, the 15 discrete velocity vectors correspond to the column vectors of the following matrix:

$$E = \begin{bmatrix} 0 & 1 & -1 & 0 & 0 & 0 & 0 & 1 & -1 & 1 & -1 & 1 & -1 & 1 & -1 \\ 0 & 0 & 0 & 1 & -1 & 0 & 0 & 1 & -1 & 1 & -1 & -1 & 1 & -1 & 1 \\ 0 & 0 & 0 & 0 & 0 & 1 & -1 & 1 & -1 & -1 & 1 & 1 & -1 & -1 & 1 \end{bmatrix} \quad (2)$$

The equilibrium distribution functions  $f_i^{\text{eq}}$  depend only on the local density and velocity and are defined in the D3Q15 model as

$$f_i^{\text{eq}} = w_i \rho \left[ 1 + \frac{3}{c^2} \mathbf{e}_i \cdot \mathbf{v} + \frac{9}{2c^2} (\mathbf{e}_i \cdot \mathbf{v})^2 - \frac{3}{2c^4} \mathbf{v} \cdot \mathbf{v} \right] \quad (3)$$

in which  $w_i$  are the weighting factors defined as

$$w_0 = \frac{2}{9}, \quad w_{1, \dots, 6} = \frac{1}{9}, \quad w_{7, \dots, 14} = \frac{1}{72} \quad (4)$$

and  $c$  is termed as the lattice speed defined as

$$c = h/\Delta t$$

with  $h$  the lattice spacing and  $\Delta t$  the discrete time step.

The computation at each time step comprises two operations: collision and streaming. The first operation simulates fluid particle collisions, which cause the fluid particles at each lattice node to scatter in different directions. The collision rules are chosen to leave the sum of the density distribution functions unchanged, or such that no fluid particle is lost. The rules are also chosen to conserve the total energy and momentum at each lattice node [15]. This computation is completely local. The second operation, streaming, is to advance the particles to the next lattice node along their directions of motion. The streaming operation takes little computational effort. These features make the LBM highly efficient, simple to implement and natural to parallelize.

The macroscopic fluid variables, density  $\rho$ , and velocity  $\mathbf{v}$  can be recovered from the distribution functions as

$$\rho = \sum_{i=0}^{14} f_i, \quad \rho \mathbf{v} = \sum_{i=1}^{14} f_i \mathbf{e}_i \quad (5)$$

In the conventional CFD methods, the pressure is typically obtained by solving the Poisson or Poisson-like equation derived from the incompressible Navier–Stokes equations that can be time consuming [17]. In the LBM, the pressure is obtained through an extremely simple equation of state,

$$p = c_s^2 \rho \quad (6)$$

where  $c_s$  is termed the fluid speed of sound and is related to the lattice speed  $c$  by

$$c_s = c/\sqrt{3} \quad (7)$$

This is an appealing feature of the LBM.

The kinematic viscosity,  $\nu$ , of the fluid is implicitly determined by the model parameters  $h$ ,  $\Delta t$ , and  $\tau$  as

$$\nu = \frac{1}{3} \left( \tau - \frac{1}{2} \right) \frac{h^2}{\Delta t} = \frac{1}{3} \left( \tau - \frac{1}{2} \right) c h \quad (8)$$

which indicates that the selection of these three parameters has to be related to each other to achieve a correct fluid viscosity.

As indicated in [12], the lattice Boltzmann equation (1) recovers the incompressible Navier–Stokes equations to the second order in both space and time [15], subject to the condition

$$Ma = \frac{v_{\max}}{c} \ll 1 \quad (9)$$

where  $Ma$  is called the ‘computational’ Mach number and  $v_{\max}$  is the maximum simulated velocity in the flow. That is, to achieve a reasonable solution accuracy, all the model parameters should be chosen in such a way that the resulting lattice speed  $c$  is sufficiently larger than the computed maximum fluid velocity. This issue has been discussed in detail in [12].

## 2.2. Turbulence modelling

While the LBM has been proven to be an efficient simulation tool for a variety of complex flow problems, the modelling of turbulent flows within the framework of the LBM is not a well investigated topic and only very limited work has been reported. However, many engineering applications are often associated with high Reynolds numbers that are turbulent in nature, particularly when particles are present. Therefore, the incorporation of a turbulence model into the LBM is essential for simulating realistic fluid–particle interaction problems.

As one of the popular turbulence modelling approaches, LES aims at directly solving large spatial-scale turbulent eddies, which carry most of the flow's energy, while using a sub-grid model to model the smaller-scale eddies. The separation of these scales is achieved through filtering the Navier–Stokes equations, from which the solutions to the resolved scales are directly obtained, while unresolved scales are modelled by sub-grid models. In this work, the widely used one-parameter Smagorinsky sub-grid model [9] is employed as the sub-grid model that assumes that the Reynolds stress tensor is dependent only on the local strain rate.

This part of the work is a straightforward extension of our previous work in two dimensions [12]. The essential steps are outlined here.

To incorporate the LES in the LBM, Equation (1) has to be modified to include the eddy viscosity, which is realized by the approach described in [18]. The filtered form of the lattice Boltzman equation [18] is expressed as

$$\tilde{f}_i(\mathbf{x} + \mathbf{e}_i \Delta t, t + \Delta t) = \tilde{f}_i(\mathbf{x}, t) - \frac{1}{\tau_*} [\tilde{f}_i(\mathbf{x}, t) - \tilde{f}_i^{\text{eq}}(\mathbf{x}, t)] \quad (10)$$

where  $\tilde{f}_i$  and  $\tilde{f}_i^{\text{eq}}$  are, respectively, the distribution function and the equilibrium distribution function at the resolved scale. The effect of the unresolved scale motion is modelled through an effective collision relaxation time scale  $\tau_t$ . Thus, in Equation (10) the total relaxation time should be changed to

$$\tau_* = \tau + \tau_t$$

where  $\tau$  and  $\tau_t$  are, respectively, the relaxation times corresponding to the true fluid (molecular) viscosity  $\nu$  and the turbulence viscosity  $\nu_*$  defined by a sub-grid turbulence model. Accordingly,  $\nu_*$  is given by

$$\begin{aligned} \nu_* &= \nu + \nu_t = \frac{1}{3} \left( \tau_* - \frac{1}{2} \right) c^2 \Delta t = \frac{1}{3} \left( \tau + \tau_t - \frac{1}{2} \right) c^2 \Delta t \\ \nu_t &= \frac{1}{3} \tau_t c^2 \Delta t \end{aligned}$$

By employing the Smagorinsky model, the turbulence viscosity  $\nu_t$  is explicitly calculated from the filtered strain rate tensor  $\tilde{S}_{ij} = (\partial_j \tilde{u}_i + \partial_i \tilde{u}_j) / 2$  and a filter length scale (the same as the lattice spacing  $h$ )

$$\nu_t = (S_c h)^2 \hat{S} \quad (11)$$

where  $S_c$  is the Smagorinsky constant; and  $\hat{S}$  the characteristic value of the filtered strain rate tensor  $\tilde{S}$

$$\hat{S} = \sqrt{\sum_{i,j} \tilde{S}_{ij} \tilde{S}_{ij}}$$

The above model is computationally very effective as  $\tilde{S}$  can be obtained directly from the second-order moments,  $\tilde{Q}$ , of the non-equilibrium distribution function

$$\tilde{S} = \frac{\tilde{Q}}{2\rho c_s^2 \tau_*} \quad (12)$$

in which  $\tilde{Q}$  can be simply computed by the filtered density functions at the lattice nodes

$$\tilde{Q}_{ij} = \sum_{k=1}^{14} e_{ki} e_{kj} (\tilde{f}_k - \tilde{f}_k^{\text{eq}}) \quad (13)$$

where  $e_{ki}$  is the  $k$ th component of the lattice velocity  $\mathbf{e}_i$ . Consequently

$$\hat{S} = \frac{\hat{Q}}{2\rho c_s^2 \tau_*} \quad (14)$$

with  $\hat{Q}$  the filtered mean momentum flux computed from  $\tilde{Q}$

$$\hat{Q} = \sqrt{2 \sum_{i,j} \tilde{Q}_{ij} \tilde{Q}_{ij}} \quad (15)$$

This approach is simple to implement as it leaves the original lattice Boltzmann equation unchanged except for the incorporation of the turbulent viscosity  $\tau_*$ .

### 3. FLUID–PARTICLE AND PARTICLE–PARTICLE INTERACTIONS

#### 3.1. Hydrodynamic forces for fluid–particle interactions

For the fluid–particle interaction problems concerned, modelling interactions between fluid and particles requires a physically correct ‘non-slip’ condition imposed on their interfaces. In other words, the fluid adjacent to the particle surface should have identical velocity as that of the particle surface. For a stationary particle, this ‘non-slip’ velocity condition can be easily achieved at the fluid–particle interface by the well-known bounce-back scheme. Assume that a particle is mapped onto the lattice by a set of lattice nodes (note that this is not a trivial issue numerically, but will not be discussed in depth here). The nodes inside and outside the solid region are, respectively, termed as solid nodes and fluid nodes. If  $i$  is a link (or direction) between a fluid node and a solid node, the bounce-back rule states that the incoming fluid particle from the fluid node is reflected back to the node it comes from, i.e.

$$f_{-i}(\mathbf{x}, t+1) = f_i(\mathbf{x}, t_+) \quad (16)$$

where  $f_i(\mathbf{x}, t_+)$  denotes the post collision distribution at the boundary node  $\mathbf{x}$  and  $-i$  is the opposite direction of  $i$ . This simple rule ensures that no tangential velocity exists along the fluid–solid interface; therefore, a ‘non-slip’ condition is imposed. Note that the particle boundary is assumed to be situated halfway between the fluid and solid node so as to achieve a second-order accuracy; otherwise, the accuracy is of first order.

It is, however, not trivial to model the interaction between the fluid and a moving particle. Ladd [4] proposed a modification to the original bounce-back rule so that the movement of a particle can

be accommodated. This approach provides a relationship of the exchange of momentum between the fluid and the solid boundary nodes. It also assumes that the fluid fills the entire volume of the particle, or in other words, the particle is modelled as a ‘shell’ filled with fluid. As a result, both solid and fluid nodes on either side of the boundary surface are treated in an identical fashion.

For a given boundary link  $i$ , the modified ‘non-slip’ rule is given by

$$f_{-i}(\mathbf{x}, t+1) = f_i(\mathbf{x}, t_+) - \alpha_i \mathbf{e}_i \cdot \mathbf{v}_b \quad (\alpha_i = 6w_i \rho / c^2) \quad (17)$$

where  $\mathbf{v}_b$  is the velocity of the middle point of the boundary link  $i$  and is computed by

$$\mathbf{v}_b = \mathbf{v}_c + \boldsymbol{\omega} \times (\mathbf{x} + \mathbf{e}_i \Delta t / 2 - \mathbf{x}_c)$$

in which  $\mathbf{v}_c$  and  $\boldsymbol{\omega}$  are, respectively, the translational and angular velocities of the particle;  $\mathbf{x}_c$  and  $\mathbf{x} + \mathbf{e}_i \Delta t / 2$  are, respectively, the particle centre and mid-boundary link coordinates.

The hydrodynamic force and torque exerted on the particle at the boundary node are computed as

$$\mathbf{F}_i = 2\mathbf{e}_i [f_i(\mathbf{x}, t_+) - \alpha_i \mathbf{e}_i \cdot \mathbf{v}_b] / \Delta t \quad (18)$$

$$\mathbf{T}_i = \mathbf{r}_c \times \mathbf{F}_i \quad (\mathbf{r}_c = \mathbf{x} + \mathbf{e}_i \Delta t / 2 - \mathbf{x}_c) \quad (19)$$

Then the total hydrodynamic forces and torque exerted on the particle are computed by summing up the forces and torques from all the related boundary links as

$$\mathbf{F} = \sum_i \mathbf{F}_i, \quad \mathbf{T} = \sum_i \mathbf{T}_i \quad (20)$$

Some other issues relevant to the modified ‘non-slip’ method have been addressed in [12]. In particular, the oscillation of the computed hydrodynamic forces on the particles promotes the choice of an alternative scheme as outlined below.

Noble and Torczynski [13] develop a moving boundary method for modelling moving obstacles in fluid flows in two dimensions. In this approach, the collision operator in the conventional LBM is modified so that it shifts smoothly between hydrodynamic at nodes occupied solely by fluid and rigid body motion at nodes occupied solely by particles. The modified collision operator make use of the fluid and solid volume fractions to weigh the corresponding portions of the collision term for nodes with both phases present.

At a lattice node, let  $h \times h \times h$  be a (cubic) nodal cell around the node and  $\gamma$  be the volume fraction of the nodal cell covered by the particle. The lattice Boltzman equation for those lattice nodes (fully or partially) covered by a solid particle is modified to enforce the ‘non-slip’ velocity condition as

$$f_i(\mathbf{x} + \mathbf{e}_i \Delta t, t + \Delta t) = f_i(\mathbf{x}, t) - \frac{1}{\tau} (1 - \beta) [f_i(\mathbf{x}, t) - f_i^{\text{eq}}] + \beta f_i^m \quad (21)$$

where  $\beta$  is a weighting function of the local fluid/solid ratio  $\gamma$  and  $f_i^m$  is an additional term that accounts for the bounce back of the non-equilibrium part of the distribution function. Three different forms of  $\beta$  and two possible formulations for  $f_i^m$  have been investigated in [13]. Their difference to the final results is generally not significant, which is also confirmed by our numerical

tests for both two-dimensional and three-dimensional analysis. The following forms of  $\beta$  and  $f_i^m$  are thus adopted in the this work:

$$\beta = \frac{\gamma(\tau - 0.5)}{(1 - \gamma) + (\tau - 0.5)} \quad (22)$$

$$f_i^m = f_{-i}(\mathbf{x}, t) - f_i(\mathbf{x}, t) + f_i^{\text{eq}}(\rho, \mathbf{v}_b) - f_{-i}^{\text{eq}}(\rho, \mathbf{v})$$

The total hydrodynamic forces and torque exerted on a particle over  $n$  particle-covered nodes are summed up as

$$\mathbf{F}_f = c h^2 \left[ \sum_n \left( \beta_n \sum_i f_i^m \mathbf{e}_i \right) \right] \quad (23)$$

$$\mathbf{T}_f = c h^2 \left[ \sum_n (\mathbf{x}_n - \mathbf{x}_c) \times \left( \beta_n \sum_i f_i^m \mathbf{e}_i \right) \right] \quad (24)$$

where  $\mathbf{x}_n$  is the coordinate of the lattice node  $n$ .

This approach has been verified for a series of two-dimensional problems including cylindrical Couette flow, sedimentation of circular and elliptical particles, and the drafting, kissing, tumbling phenomenon [19]. Recently, the method has also been verified for several problems in three dimensions such as a moving sphere in creeping Poiseuille flow and a settling sphere in a column of fluid [14]. These validations demonstrate that the moving boundary condition described above is capable of accurately computing the forces and torques acting on solid particles.

### 3.2. Contact forces for particle–particle interactions

In many lattice Boltzmann simulations of particle–fluid problems, the inter-particle interaction is either ignored or treated in a simple manner. However, many practical applications require accurate resolutions of the particle contact. A rational choice is to employ the DEM to account for this interaction.

The DEM has become a promising numerical tool capable of simulating problems of a discrete or discontinuous nature. It was originated in geotechnical and granular flow applications in the 70s by Cundall and Strack [20]. In its framework, a discrete system is considered as an assembly of individual discrete objects that are treated as rigid and represented by discrete elements as simple geometric entities. The dynamic response of discrete elements depends on the interaction forces between them, which can be short-ranged, such as mechanical contact, and/or medium-ranged, such as attraction forces in liquid bridges, and obey Newton's second law of motion. By tracking the motion of individual discrete objects, the dynamic behaviour of a discrete system can be simulated. In addition to simple geometrical entities such as spheres, more complex-shaped elements such as polyhedra and clusters of spheres can also be used to represent realistic objects encountered in practical applications. The dynamic equations of the discrete system are normally solved numerically by the central difference-based explicit integration scheme at discrete time instants.

The solution procedure involved in the DEM at each time step consists of (1) (global) spatial search, (2) (local) interaction resolution, (3) interaction force computation, and (4) solutions of element positions and velocities. In the global search phase, a list of neighbouring elements that may potentially interact with each discrete element is determined. Over the last decade, significant

progress has been made in the development of highly effective search algorithms capable of dealing with a large numbers of discrete objects (several millions, for instance). See [21] for a comprehensive review and performance comparison for a number of commonly used tree-based and cell-based search algorithms. In the local resolution phase, the pairs in potential contact identified from the global search are subjected to kinematic resolutions based on their actual geometric shapes. If the pairs are in contact, interaction forces need to be computed according to certain constitutive relationship or interaction law. This is the third phase. When all the forces acting on the discrete elements are computed, the displacements, velocities, and accelerations of the global system at the time instant are updated in the solution phase using the central difference time stepping scheme. These computations are repeated for every time step throughout the simulation. However, the global search is performed when necessary.

Note that in the DEM, the contact between discrete objects is simulated along their boundaries by appropriate penalty-based interaction laws, which essentially govern the relation of the distance of the relative approach or overlap, and the generated repulsive force between the contacting pairs. Discrete objects are considered to be rigid, but a certain small overlap between discrete objects is allowed, i.e. a ‘soft’ model [22] is adopted. This ‘soft’ model may be justified by the fact that discrete objects are physically deformable and thus the allowed overlap may partially offset the error introduced by the assumed rigidity of the discrete objects. Furthermore, it is assumed that the overlap is sufficiently small for small deformation theory to be applicable when describing the deformation of the contacting region of discrete objects. If  $\delta$  denotes the maximum contact overlap (or penetration), this small contact deformation assumption requires that  $\delta \ll 2R$ , where  $R$  is the radius of a sphere or the characteristic length of an irregular-shaped particle. The interaction laws should correctly represent the physical relationship between the interaction forces and the contact overlap or characteristics.

For the current problem, each particle is represented by a spherical discrete element. A linear or Hertz contact model is employed for the normal contact between a contact pair, while the frictional forces are computed with the modified Coulomb friction law, although it is considered not important for the problem concerned. A detailed discussion of the contact interaction laws can be found in [23]. Note that the lubrication pressure developed between two approaching particles is not considered here, which may be important for some applications.

### 3.3. LBM and DEM coupling

Fluid and particle coupling at each time step is realized by first computing the fluid solution and then updating the particle positions through the integration of the equations of motion given by

$$\begin{aligned} \mathbf{m}\mathbf{a} + \mathbf{c}\mathbf{v} &= \mathbf{F}_c + \mathbf{F}_f + \mathbf{m}\mathbf{g} \\ \mathbf{J}\ddot{\boldsymbol{\theta}} &= \mathbf{T}_c + \mathbf{T}_f \end{aligned} \quad (25)$$

where  $\mathbf{m}$  and  $\mathbf{J}$  are, respectively, the matrices of the mass and the moment of inertia of the particle,  $\ddot{\boldsymbol{\theta}}$  the angular acceleration vector,  $\mathbf{g}$  the gravitational acceleration if considered,  $\mathbf{F}_f$  and  $\mathbf{T}_f$  are, respectively, the hydrodynamic force and torque vectors,  $\mathbf{F}_c$  and  $\mathbf{T}_c$  denote the contact force and torque vectors from particle–particle and particle–boundary walls,  $\mathbf{c}$  is a damping matrix, and the term  $\mathbf{c}\mathbf{v}$  represents a viscous force vector that accounts for the effect of all possible dissipation forces in the system. The static buoyancy force of the fluid is taken into account by reducing the gravitational acceleration to  $(1 - \rho/\rho_s)\mathbf{g}$ , where  $\rho_s$  is the density of a particle.

The time step used in the time integration of (25) should be appropriately selected to satisfy the solution accuracy requirement and more importantly to ensure numerical stability due to the explicit nature of the central difference algorithm. For a local linear normal contact model

$$F_c = k_n \delta \tag{26}$$

where  $k_n$  is the normal stiffness and  $\delta$  the penetration; the critical time step for the central difference algorithm is given by

$$\Delta t_{cr} = 2(\sqrt{1 + \xi^2} - \xi) / \omega \tag{27}$$

where  $\omega = \sqrt{k_n/m}$  is the local contact natural frequency and  $\xi$  is the critical damping ratio. As pointed out [24], this critical time value may be too large for impact systems. Thus, the actual time step used for the integration of Equation (25) is taken as

$$\Delta t_D = \lambda \Delta t_{cr} \tag{28}$$

where the time step factor  $\lambda$  is normally chosen to be around 0.1.

When the dynamic equation (25) governing the evolution of the particle–fluid system is solved by the explicit central difference scheme, there are two computational issues that are worth mentioning below, although the same issues have been discussed in [12].

(1) *Sub-cycling time integration:* There exist two different time steps in the combined LBM–DEM solution procedure:  $\Delta t$  for the fluid flow and  $\Delta t_D$  for the discrete particles. At least for the problem concerned,  $\Delta t_D$  is smaller than  $\Delta t$ . One solution would be to set  $\Delta t = \Delta t_D$ . However, it is not a viable option since  $\Delta t_D$  is dynamically changing and  $\Delta t$  is implicitly determined by the grid size  $\Delta x$ , the relaxation time  $\tau$ , and the viscosity of the fluid. A more feasible option is to reduce  $\Delta t_D$  to a new  $\Delta t_s$  so that the ratio between  $\Delta t$  and  $\Delta t_s$  is an integer  $n_s$ :

$$\Delta t_s = \frac{\Delta t}{n_s} \quad (n_s = \lceil \Delta t / \Delta t_D \rceil + 1) \tag{29}$$

where  $\lceil \cdot \rceil$  denotes an integer round-off operator. This essentially leads to a so-called sub-cycling time integration scheme: in one step of the LB fluid computation,  $n_s$  sub-steps of integration are performed for the discrete part using the time step  $\Delta t_s$ ; while the hydrodynamic forces  $\mathbf{F}_f$  and  $\mathbf{T}_f$  are kept unchanged during the sub-cycling.

(2) *The dynamic equations in the lattice coordinate system:* Since all the lattice Boltzman-related equations are implemented in the lattice coordinate system in this work, the dynamic equation (25) should be implemented in the same consistent manner. Equation (25) in the lattice coordinate system takes the form of

$$\bar{\mathbf{m}}\bar{\mathbf{a}} + \bar{\mathbf{c}}_d\bar{\mathbf{v}} = \bar{\mathbf{F}}_c + \bar{\mathbf{F}}_f + \bar{\mathbf{m}}\bar{\mathbf{g}} \tag{30}$$

where

$$\begin{aligned} \bar{\mathbf{m}} &= \mathbf{m} / \rho_s h^3, & \bar{\mathbf{v}} &= \mathbf{v} / c \\ \bar{\mathbf{a}} &= \mathbf{a} \Delta t / c, & \bar{\mathbf{g}} &= \mathbf{g} \Delta t / c \\ \bar{\mathbf{c}}_d &= ch\mathbf{c}_d, & \bar{\mathbf{F}}_f &= \mathbf{F}_f / (\rho_0 c^2 h^2) \end{aligned}$$

Table I. Particle size distribution.

Particle size (mm)	Distribution (%)	Cumulative (%)
12	10	100
10	40	90
8	40	50
6	10	10

and  $\bar{\mathbf{F}}_c$  is the scaled contact force. For a linear normal contact model,

$$\bar{\mathbf{F}}_c = \bar{k}_n \bar{\delta}, \quad \bar{k}_n = k_n / c^2 h$$

Then the scaled natural frequency  $\bar{\omega}$ , the critical time step  $\bar{\Delta}t_{cr}$ , and the time step  $\bar{\Delta}t_s$  are respectively taken as:

$$\bar{\omega} = \omega \Delta t, \quad \bar{\Delta}t_{cr} = \Delta t_{cr} / \Delta t, \quad \bar{\Delta}t_s = 1 / n_s$$

#### 4. EXPERIMENTAL COMPARISON

To assess the solution accuracy and performance of the combined three-dimensional LBM–DEM approach proposed in the preceding sections, a much simplified laboratory testing of vacuum dredging systems for mineral recovery is conducted elsewhere. Experimental results obtained can be utilized to compare with the numerical simulation and thus provide, to a certain extent, an indication of the solution accuracy of the combined LBM–DEM with the Smagorinsky turbulent model for fluid particle problems.

A vacuum dredging system for mineral recovery is of practical importance in the mining industry. This recovery operation employs a suction process to extract rock fragments. It consists of a rigid pipe connected to a slurry transport system, which is typically powered by a gravel pump, although other types of pumping systems can be used. The gravel is transported to the pipe entrance via hydraulic entrainment. Effective computer modelling techniques are sought to assist and optimize the design of this operation.

##### 4.1. Experimental setup

The experimental setup for a simplified system consists of a Perspex suction pipe connected to a positive displacement pump via a flexible pipe, with the inlet of the suction pipe being held at a fixed distance from the gravel surface. The distance above the gravel surface will be referred to as the stand-off distance (SOD). The pump is started once the SOD has been fixed, and the test is considered complete when gravel entrainment has stopped.

The suction pipe has an internal diameter of 101 mm, a tube thickness of 16 mm, and is made of Perspex. The gravel is initially confined to a cylindrical region called the gravel bed of 300 mm in diameter and 70 mm in depth. The gravel particles are made of quartz with a density of  $\rho = 2650 \text{ kg/m}^3$ , and are assumed to be spherical with diameter in the range of 6–12 mm. Table I lists the particle size distribution. The particles are randomly packed, having an initial porosity of approximately 50%.

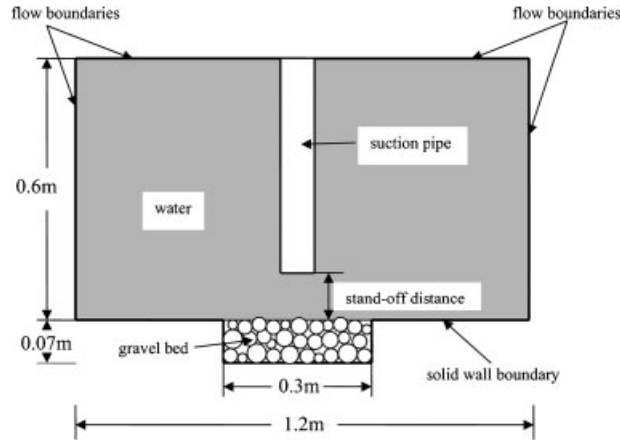


Figure 2. The front view of the problem geometry.

The flow inside the suction pipe is expected to be fully turbulent. The fluid is water. Both water and gravel particles are initially at rest.

During the test, video footage is captured using a high-speed digital camera. Image processing is used to provide an indication of the gravel velocity history during the test. The final excavation profile and gravel volume removed during the test are also recorded.

#### 4.2. Computational setup

From the experimental results, it is clear that particles are only entrained in a limited region around the pipe entrance. It is therefore reasonable to assume that the gravel particles are restricted to a cylindrical region that is larger than the entrainment zone, and that the effect of the far field particles can be ignored so that a less number of discrete particles need to be modelled. The front view of the idealized problem geometry is shown in Figure 2.

The combined three-dimensional LBM–DEM procedure, described in the previous section, is then implemented for stand-off distances  $SOD = 0$  and 30 mm, respectively.

A total of 5086 spheres with the same size distribution as that of the experiment (as shown in Table I) are randomly positioned at gravel bed, using the packing algorithm developed in [25]. Full gravity ( $g = 9.81 \text{ m/s}^2$ ) is applied. The moving boundary method of Noble and Torczynski [13] is employed to compute the fluid–particle interaction forces. Different versions of the method are compared and no significant difference is observed. The linear sphere/sphere and sphere/facet contact models are used to model the normal contact between the particles and between particles and boundary walls, while the frictional contact is neglected. The LES-based Smagorinsky turbulence model is adopted with the Smagorinsky constant  $S_c = 0.1$ . The following parameters are chosen: particle density  $\rho_s = 2650 \text{ kg/m}^3$ , normal contact stiffness  $k_n = 5 \times 10^8 \text{ N/m}$ , contact damping ratio  $\xi = 0.5$ , and time step factor  $\lambda = 0.1$ , which gives a time step of  $\Delta t_D = 1.16 \times 10^{-5}$  for the DEM simulation of the particles. The fluid domain is divided into regular lattice with lattice spacing  $h = 2.5 \text{ mm}$ . The fluid properties are those of water at room temperature, i.e. density  $\rho = 1000 \text{ kg/m}^3$  and kinematic viscosity  $\nu = 10^{-6} \text{ m}^2/\text{s}$ . A complete simulation is achieved with  $\tau = 0.50002$ . This gives a time step  $\Delta t = 4.17 \times 10^{-5} \text{ s}$  and thus the corresponding lattice speed  $c = 60 \text{ m/s}$ .

The boundary conditions are set as follows. Except for the bottom of the gravel bed, which is a solid stationary wall, the others are flow boundaries. A constant pressure boundary condition with  $\rho_{\text{in}} = \rho$  is imposed at the inlet walls, and a smaller pressure with  $\rho_{\text{out}} = 0.975\rho$  is applied to the outlet of the pipe. The flow is therefore driven by the pressure difference between the inlet and outlet.

#### 4.3. Comparison of computational and experimental results

Figure 3 shows the images of the gravel motion at the start, during, and towards the end of the experiment and simulation, respectively.

Of greater importance are the flow velocity at the pipe outlet, the total weight of the gravel particles removed, and the excavation profile. The calculated values are compared with those observed from experimentation. For  $\text{SOD} = 0$ , the predicted average velocity on the exit plane of the suction pipe is approximately 0.99 m/s, which agrees well with the measured value (1.05 m/s). A volume of 678 341 mm<sup>3</sup> of gravel is removed in the test, which weighs approximately 1.09 kg (assuming a bulk density of 1600 kg/m<sup>3</sup>), while 1110 particles, weighting 1.22 kg in total, are excavated in the simulation.

The final excavation profiles, measured, respectively, from the experimentation and simulation, at the gravel bed are illustrated in Figure 4. The excavation profile from the experiment is obtained from a randomly selected cross section of the bead, while the profile for the simulation is obtained by a radial mapping of all the particles onto the cross section and then rotating about the central axis to create an axisymmetrical profile to facilitate the comparison with the experiment. Similarity of the two profiles is clearly evident although no quantitative comparison is made. Note that the detail of the pebble bed structure is not important for the comparison purpose.

The simulated maximum fluid velocity is  $v_{\text{max}} = 1.36$  m/s at the pipe outlet (with the characteristic length  $L = 0.101$  m). Thus, the maximum Mach number and Reynolds number are, therefore, estimated as

$$Ma = \frac{v_{\text{max}}}{c} = 0.0226$$

$$Re = \frac{v_{\text{max}}L}{\nu} = 137\,360$$

The Mach number indicates that the results obtained are reasonably accurate. See [12] for the detail.

For  $\text{SOD} = 30$  mm, none of the particles were removed in the simulation, as is the case in the experiment. It can be seen that the overall correspondence between numerical results and experimental measurements is good.

## 5. CONCLUSIONS

This paper introduces a combined three-dimensional lattice Boltzmann and discrete element solution strategy for numerical simulations of fluid–particle interaction problems. The fluid field is solved by the extended lattice Boltzmann equations with the incorporation of the Smagorinsky turbulence approach, while particle interactions are modelled by the DEM. The hydrodynamic interactions between fluid and particles are realized through the three-dimensional generalization

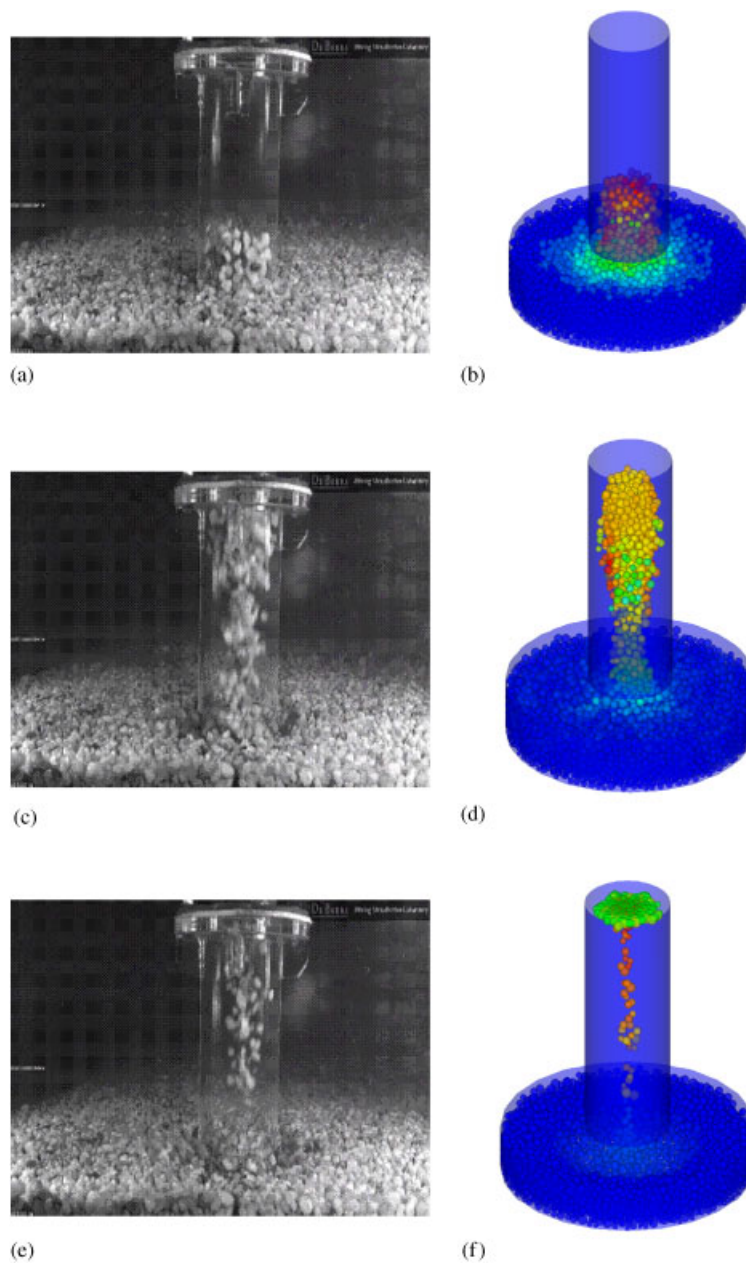


Figure 3. Images of gravel motion at different stages of experiment and simulation: (a) gravel motion at the start of the test; (b) gravel motion at the start of the simulation; (c) gravel motion during the test; (d) gravel motion during the simulation; (e) gravel motion towards the end of the test; and (f) gravel motion towards the end of the simulation.

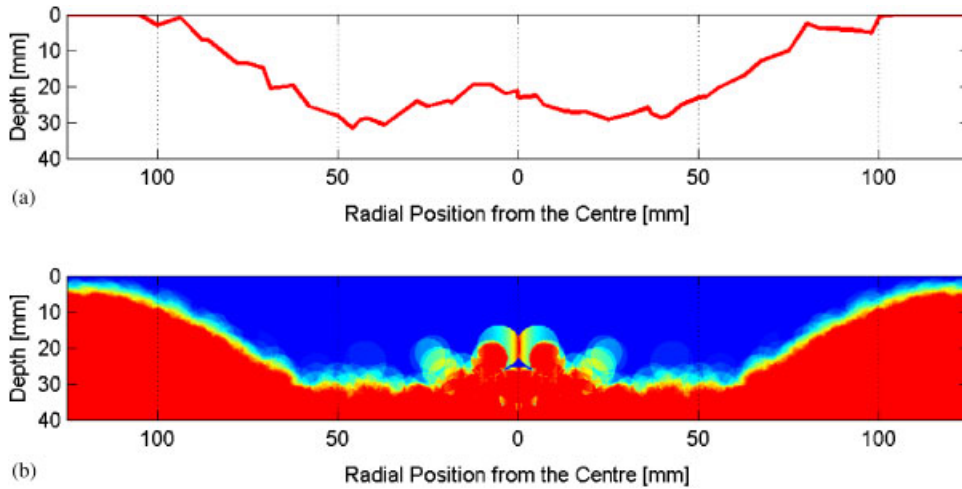


Figure 4. Excavation profiles of the experiment and simulation: (a) excavation profile of the test and (b) excavation profile of the simulation.

of a scheme proposed by Noble and Torczynski [13], which leads to a combined procedure for modelling three-dimensional fluid–particle interactions. The main computational aspects comprise the lattice Boltzmann formulation for the solution of fluid flows, the incorporation of the large eddy simulation-based turbulence model within the framework of the LBM for turbulent flows, the three-dimensional moving boundary condition for hydrodynamic interactions between fluid and moving particles, and the discrete element modelling of the interaction between particles. The numerical simulations against experimentation demonstrate that the proposed approach is a promising computational tool capable of simulating practical fluid–particle interaction problems with a large number of moving particles and high Reynolds numbers.

#### ACKNOWLEDGEMENTS

The first author is very grateful for partial support by a Leverhulme Trust Research Fellowship Award (No. RF/9/RFG/2007/0326).

#### REFERENCES

1. Kuipers J, van Duin K, van Beckum F, van Swaaij W. A numerical model of gas-fluidized beds. *Chemical Engineering Science* 1992; **47**:1913–1924.
2. Tezduyar TE. Finite element methods for flow problems with moving boundaries and interfaces. *Archives of Computational Methods in Engineering* 2001; **8**(2):83–130.
3. Chen H, Kandasamy S, Orszag S, Shock R, Succi S, Yakhot V. Extended Boltzmann kinetic equation for turbulent flows. *Science* 2003; **301**:633–636.
4. Ladd A. Numerical simulations of fluid particulate suspensions via a discretized Boltzmann equation (Parts I and II). *Journal of Fluid Mechanics* 1994; **271**:285–339.
5. Aidun CK, Lu Y, Ding E-G. Direct analysis of particulate suspensions with inertia using the discrete Boltzmann equation. *Journal of Fluid Mechanics* 1998; **373**:287–311.
6. Feng ZG, Michaelides EE. Proteus: a direct forcing method in the simulations of particulate flows. *Journal of Computational Physics* 2005; **202**:20–51.

7. Nguyen N, Ladd A. Sedimentation of hard-sphere suspensions at low Reynolds number. *Journal of Fluid Mechanics* 2005; **525**:73–104.
8. Qi D, Luo L. Rotational and orientational behaviour of three-dimensional spheroidal particles in Couette flows. *Journal of Fluid Mechanics* 2003; **477**:210–213.
9. Smagorinsky J. General circulation experiments with the primitive equations. I. The basic experiment. *Monthly Weather Review* 1963; **91**(3):99–164.
10. Latt J, Chopard B, Succi S, Toschi F. Numerical analysis of the averaged flow field in a turbulent lattice Boltzmann simulation. *Physica A: Statistical Mechanics and its Applications* 2006; **362**(1):6–10.
11. Han K, Feng YT, Owen DRJ. Numerical simulations of irregular particle transport in turbulent flows using coupled LBM–DEM. *Computer Modeling in Engineering and Science* 2007; **18**(2):87–100.
12. Feng YT, Han K, Owen DRJ. Coupled lattice Boltzmann method and discrete element modelling of particle transport in turbulent fluid flows: computational issues. *International Journal for Numerical Methods in Engineering* 2007; **72**(9):1111–1134.
13. Noble D, Torczynski J. A lattice Boltzmann method for partially saturated cells. *International Journal of Modern Physics C* 1998; **9**:1189–1201.
14. Erik Strack O, Cook BK. Three-dimensional immersed boundary conditions for moving solids in the lattice-Boltzmann method. *International Journal for Numerical Methods in Fluids* 2007; **55**:103–125.
15. Chen S, Doolen G. Lattice Boltzmann method for fluid flows. *Annual Review of Fluid Mechanics* 1998; **30**:329–364.
16. Bhatnagar PL, Gross EP, Krook M. A model for collision processes in gases. I. Small amplitude processes in charged and neutral one-component systems. *Physical Review* 1954; **94**:511–525.
17. Mei R, Luo L, Shyy W. An accurate curved boundary treatment in the lattice Boltzmann method. *Journal of Computational Physics* 1999; **155**:307–330.
18. Yu H, Girimaji S, Luo L. DNS and LES of decaying isotropic turbulence with and without frame rotation using lattice Boltzmann method. *Journal of Computational Physics* 2005; **209**:599–616.
19. Cook BK, Noble DR, Williams JR. A direct simulation method for particle–fluid systems. *International Journal for Engineering Computations* 2004; **21**(2–4):151–168.
20. Cundall PA, Strack ODL. A discrete numerical model for granular assemblies. *Geotechnique* 1979; **29**(1):47–65.
21. Han K, Feng YT, Owen DRJ. Performance comparisons of tree based and cell based contact detection algorithms. *International Journal for Engineering Computations* 2007; **24**(2):165–181.
22. Cundall PA, Hart RD. Numerical modelling of discontinua. *International Journal for Engineering Computations* 1992; **9**:101–113.
23. Han K, Perić D, Owen DRJ, Yu J. A combined finite/discrete element simulation of shot peening process. Part II: 3D interaction laws. *International Journal for Engineering Computations* 2000; **17**(6/7):684–702.
24. Feng YT. On the central difference algorithm in discrete element modeling of impact. *International Journal for Numerical Methods in Engineering* 2005; **64**(14):1959–1980.
25. Han K, Feng YT, Owen DRJ. Sphere packing with a geometric based compression algorithm. *Powder Technology* 2005; **155**(1):33–41.